Magic Analyzer Simulation Report

Erik Bergbäck Knudsen

August 2020

This is the report document where the studies performed with the McStas component `Pol_straight_tapering`developed for the Magic Analyzer project will be detailed.

1 Introduction

PSI are building a wide-angle analyzer for the MAGiC-instrument at ESS as a in-kind contribution. As part of this DTU and PSI have entered into a collaboration for supporting this work with computer simulations. At a kick-off meeting at PSI we decided that a new component for McStas[2] was to be developed, and a set of basic simulation runs were to be done to determine parameters such transmission, polarizing power, etc.

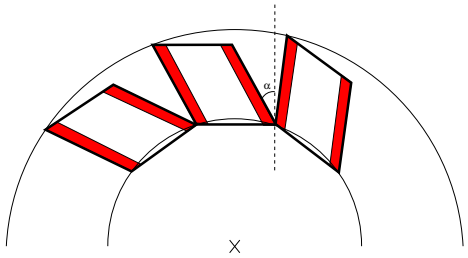

Figure 1: Sketch of the geometry of three channels. The tilt angle α is indicated. As the channels have parallel walls, a gap forms on the exit side. The supermirror coating is indicated in red. Not that the blades are considered skew as opposed to simply angled square blades, which is the real geometry.

The considered analyzer concept is a solid-state analyzer where neutrons are propagated *inside* vertical Si-plates. The plates are coated with polarizing FeSi-supermirror coatings on both sides on top of which an absorbing Gd-layer is deposited. Thus, only a single spin-state is reflected and guided through the plate, the other is absorbed in the Gd (after being transmitted through the supermirror). To avoid direct line of sight, the blades should be tilted by an angle, α,. Ideally this should be a constant angle, but naturally some amount of misalignment is to expected.

The complete analyzer will cover $\beta = 120°$, but to start the project PSI have built a prototype version which has 1.875° coverage. It is apparent from the physical device that the plates get curved from stress originating from the coating. Important features to study are the basic parameters, but also misalignment effects.

The report will deal with the following things: Section 2 describes the logic followed in the component, section 3 the testing runs we have performed to verify that the component code works. Section 4 is set of tests that validate the simulations against a set of measurements on the prototype analyzer performed at BOA. Section 5.1 is a study on the effect of analyzer misalignment, whereas section 6 describes an simulation campaign for building a complete MAGiC model, including the full version of the analyzer.

2 Component logic

Geometry simplification: The channels/plates are skewed, not angled as they would be in a real device. This should be a relatively simple fix to make in the component (see fig. 1).

In the initialize section we compute cross sections from material parameters, and read data files containing reflectivity and optionally plate misalignment.

The overall ray trace algorithm, in the newly developed component: `Pol_straight_tapering`, is briefly as follows:

1. Transport the ray to the entry of the component. If the parameter entry_radius is > 0 the analyzer is an arc, otherwise it is considered flat. At present the flat entry option is not supported however, as it was deemed uninteresting for this particular project.

2. At the entry, we check if the ray is within the bounds of the analyzer, if it is we set SCATTER; if not it is left alone? As SCATTER is set we may use that in an EXTEND to emulate an absorbing entry aperture.

3. Given channel thickness and coating thicknesses, we determine which channel the ray hits, and compute the outer coordinates (including coatings) of that channel.

4. Compute coordinates for the entry side corners of the channel proper and coatings (see section 2.1). If `abs_flag` is set anything hitting the supermirror coating from the side is ABSORBED.

5. By the corners and the parameter alpha (tilt angle) we may determine the normal vector(s) of the side walls. Once they are in place we enter a loop. At this point an extra angle dalpha may be added to alpha due to misalignment. This is done through a table lookup in a datafile.

   (a) For each loop iteration we check the intersection times of side wall planes, top and bottom planes, and exit plane, and find the smallest positive intersection time.

(b) If either exit, top or bottom is smallest the neutron we propagate to the intersection point exit the loop. If either of the side wall intersections are hit first, we transport the neutron to intersection point, and reflect it the wall normal.

(c) Apply reflectivity to the neutron ray weight, by a table lookups for spin-up and spin-down. The ratio with which these apply depend on what the polarization of the ray is at this point. Polarization perpendicular to the the polarizing direction of the supermirror will be converted into loss of reflectivity.

(d) The neutron is now propagated a tiny bit, to avoid re-reflection in the next iteration due to numerical precision.

(e) The loop is continued unless a threshold value of iterations is overrun.

6. At each propagation inside the loop the propagation length is summed. After exiting the loop attenuation according to cross sections of the plate material (e.g. Si) is applied to the ray weight, and control of the ray is relinquished.

2.1 Supermirror edges

If the supermirror layer thickness is not negligible, there is a finite possibility that a ray will enter it from the side. The physics inside the supermirror is considered to be out of scope of this study. The situation could be considered analogous to losses inside coatings for neutrons guide which has been explored in [1], and possibly the techniques used for that study could be employed here if a closer study is warranted. For this study we will investigate the effect by developing upper and lower bound estimates, using the following logic: If a ray hits the supermirror edge its further destiny depends on the flag **abs_flag**. If the parameter is set ($\neq 0$) the ray is simply terminated as if it had hit the absorbing Gd-layer. If the flag is *not* set a few things can happen (fig. 2).

case a: The ray exits the supermirror on a trajectory into the channel. The ray will be transported into the channel as if the supermirror had been part of the plate. I.e. absorption and scattering corrections are applied along the way through the supermirror. It also applies the reflectivity R(Q=0) to the ray at the 1st interface.

case b: The ray stays inside the supermirror layer for the length of the plate, on an outward trajectory, i.e. towards the absorbing layer. The ray will be terminated as if it had hit the absorbing layer.

case c: The ray stays inside the supermirror layer for the length of the plate, on an inward trajectory, i.e. towards the channel. The ray will be transmitted as if the supermirror had been part of the channel.

case d: The ray exits the supermirror through the Gd-layer. The ray is terminated.

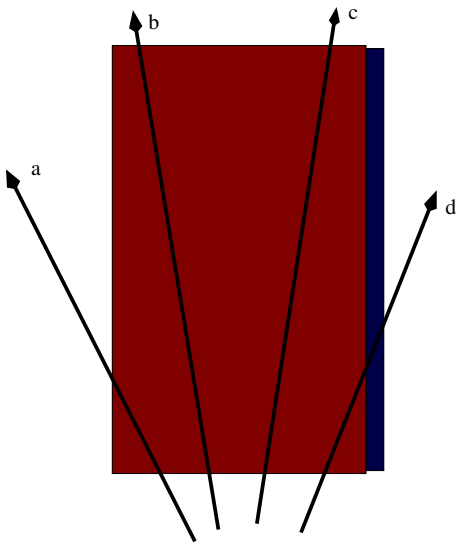

Figure 2: Sketch of the different logical cases that arise when a ray hits the supermirror edge. The dark red area represents the supermirror coating, the dark blue the absorbing Gd-layer. Thus Si-plate is to the of the dark red area. Trajectories a through d denote the logical cases that apply when a ray hits the supermirror coating from the edge.

We quantify the significance pf this parameter by simply running a simulation twice

The expactation was that the significance of the **abs_flag** parameter is small

3 Component testing

First, let the channel walls be completely absorbing, and set the tilt angle, α, to 0. In this parameterization the analyzer acts as a radial collimator. Note that the channels are of constant width (see fig. 1) which will results in gaps between the channels on the exit end. Further, let the channel width be driven by a set number of channels, and angle of coverage, β. Place a perfect point source in the analyzer centre. Figure 3 shows the normalized intensity profile for a set of channel/plate widths. Qualitatively, this is exactly the expected behaviour.

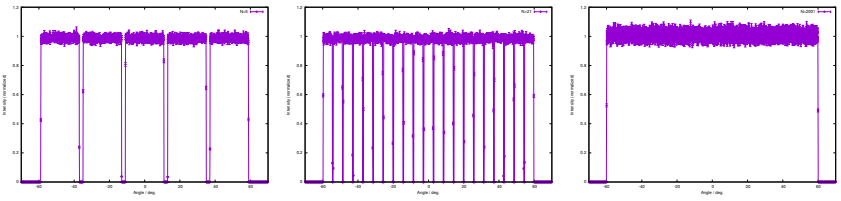

Figure 3: Intensity transmission profile as a function of angle, when using the wide angle analyzer model as a collimator, i.e. with absorbing walls and tilt angle 0 deg. Left: 5 channels/blades. Middle: 21 channels. Right: 2001 channels.

In the case of 2001 channels no gaps are visible between the blades, but this is merely due to the binning of the monitor being larger than the blade width.

As a further unit test we may look at the central angle 0 deg. Here should directly be able to read off the absorption of the Si-blade.

$$I/I0 = e{-}\mu l; \quad \mu_{total} = \mu_{abs} + mu_s; \quad ;\mu_{abs} = \frac{2200}{v}\sigma_{abs}\rho N_A/A_t \qquad (1)$$

In our test examples blades were $l = 0\,1m$, made from Si with literature values of: $rho = 2.33\,\mathrm{g/cm^3}, A_t = 28.09\,\mathrm{g/mol}, \sigma_{abs} = 0.171$ barns. For simplicity, in this 1st test we have simply ignored the coherent and incoherent scattering, which obviously should be taken into account in any "real" examples. With a wavelength $\lambda = 4\,$Å, from the central bin at $\theta = 0°$ we can recover $\mu_{abs} = 1.8996\,$/m compared with the theoretical $\mu_{abs} = 1.8994\,$/m. https://www.overleaf.com/project/5e4a6175b74bb800011b2e4a

Now view the analyzer transmission as a function of α: If the source is a point, the direct line of sight is lost when:

$$\sin(\alpha)l \geq 2R\sin\left(\frac{\beta}{2N}\right) + \cos(\alpha)l\tan\left(\frac{\beta}{2N}\right) \qquad (2)$$

at equality this turns into:

$$\sin(\alpha)l = 2R\sin\left(\frac{\beta}{2N}\right)+\cos(\alpha)l\tan\left(\frac{\beta}{2N}\right) \rightarrow sin\alpha \approx \frac{2R}{l}\sin\left(\frac{\beta}{2N}\right)+\tan\left(\frac{\beta}{2N}\right) \quad (3)$$

In the example with a full width analyzer, $\beta = 120°$ and absorbing wall this would mark the spot when the transmission of the device drops to 0. Figure 4 left, shows a scan of the α angle. The theoretical value given by eq. (3) for a device with 501 channels we find to be: $\alpha = 2.51°$. The conclusion is that the α angle logic works as expected.

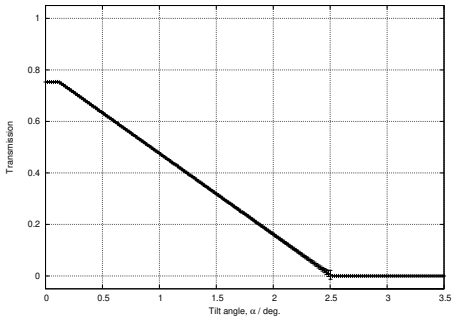

Figure 4: Left: Transmission as a function of tilt angle alpha for a $\beta = 120°$ analyzer, with 501 Si-blades, and total absorbing side walls. At $\alpha \approx 2.5°$ the transmission reaches 0.

4 Modeling the PSI-built prototype of the analyzer

A scaled down version of the analyzer was realized at the sputtering lab at PSI. Initially, the prototype was to have coverage of 2.5° consisting of 4 packets of 63 blades each. All blades were coated with a m=3.2 Fe/Si polarizing supermirror, 4 µm thick, on both sides. On top of this a 0.8 µm Gd absorber layer was added. The entry radius of curvature was 0.9 m and the blade length was length=0.04 m (parameters summarized in table 1). Due to engineering problems, the prototype was scaled down a biut further to have on 3 packets of 62 blades, which leads to an angle coverage of 1.875°.

With these parameters in place, we can now turn to the effect of the supermirror width on the analyzer transmission. Figure 5 shows transmission and polarization of a fully (radially) illuminated prototype, with idealized reflectivity and with the **abs_flag** turned off (= 0) and on (= 1). To provide a clear conclusion on the edge effect, the analyzer was illuminated by a point

coverage, β	1.875°
no. blades	3×62
blade thickness	150 µm
supermirror coating	FeSi, 4 µm
absorption coating	Gd, 0.8 µm
entry curvature radius	0.9 m
length	4 mm

Table 1: Parameters of the PSI MAGiC-analyzer prototype.

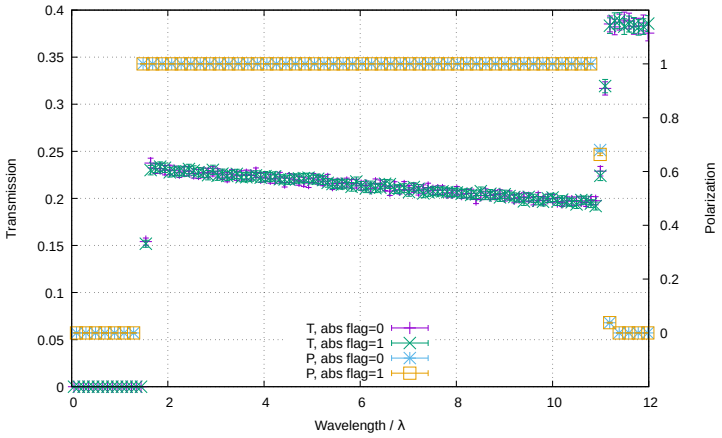

Figure 5: Transmission and Polarization for the PSI prototype (table 1) illuminated by a point source for absorption flag off (= 0) and on (= 1).

source, fully illuminating the analyzer width with a uniform wavelength spectrum. As expected there is little to no difference between the two modes, and thus we conclude that with a ratio between coating and blade width as here: $\frac{d_{sm}}{d_{ch}} = \frac{4.8}{150} \approx 0.032$, the supermirror edge effect is negligible.

The reflectivity of the coating has been measured at PSI (fig. 6). Such measures values are simply read and stored in memory by the component code. For q-values between the data points in the table we rely on linear interpolation.

4.1 Ideal vs. real reflectivity

To assess the effect of the reflectivity of the blades we have performed a few simulations using both the a reflectivity fitted to measured reflectivities through the standard neutron reflectivity function: (eq. (4)) and also an idealized dataset with only reflectivity 0 and 1, where the q-values for the transition transitions roughly match those of the measured curves (fig. 6). The resulting fit-parameters may be found intable 2

$$R(q) = R_0 \frac{1}{2}\left(1 - \tanh\left(\frac{q - m * q_c}{W}\right)\right)(1 - \alpha\,(q - q_c)) \tag{4}$$

spin state	R_0	q_c	α	m	W
up	0.995	0.0254	11.472	2.78	0.00108
down	0.995	0.0124	0	1	0.00484

Table 2: Fitted parameters to the standard function: eq. (4), for the reflectivity curves in fig. 6.

We note some points about fig. 6. First, that the reflectivity is sometimes > 1, which is clearly unphysical, but also within the overall fluctuations of the curves. Second, we note a drop a reflectivity for low q. This is attributed to measurement difficulties at low angles, where the beam footprint can exceed the plate length. Third, the low q drop makes a fit of q_c unreliable. To avoid this we have fixed q_c to the theoretical values for Fe: $q_{c,up} = 0.0254 \quad q_{c,down} = 0.0124$.

A comparison of analyzer performance between fitted ideal reflectivities is shown in figs. 7 to 8. As expected, the differences are minor, but there are a few details worth mentioning:

- For $\lambda \approx 1.0$, fig. 8 appears to suggest that the analyzer with fitted reflectivity works fine, whereas the ideal one does not. From fig. 7 we can see that although the polarization power is perfect, there is very little transmission in this range. Since $R_{up} << 1$, throughput is very limited, but since $R_{up} > Rdown$ also above the cut-off, the small remaining intensity is polarized nontheless.
- Figure 7 shows a splitting of the curves in the transition range, which obviously is invisible in fig. 8. This effect has not been studied closer. Our initial guess is that this is an effect of the discrete orders of reflections.

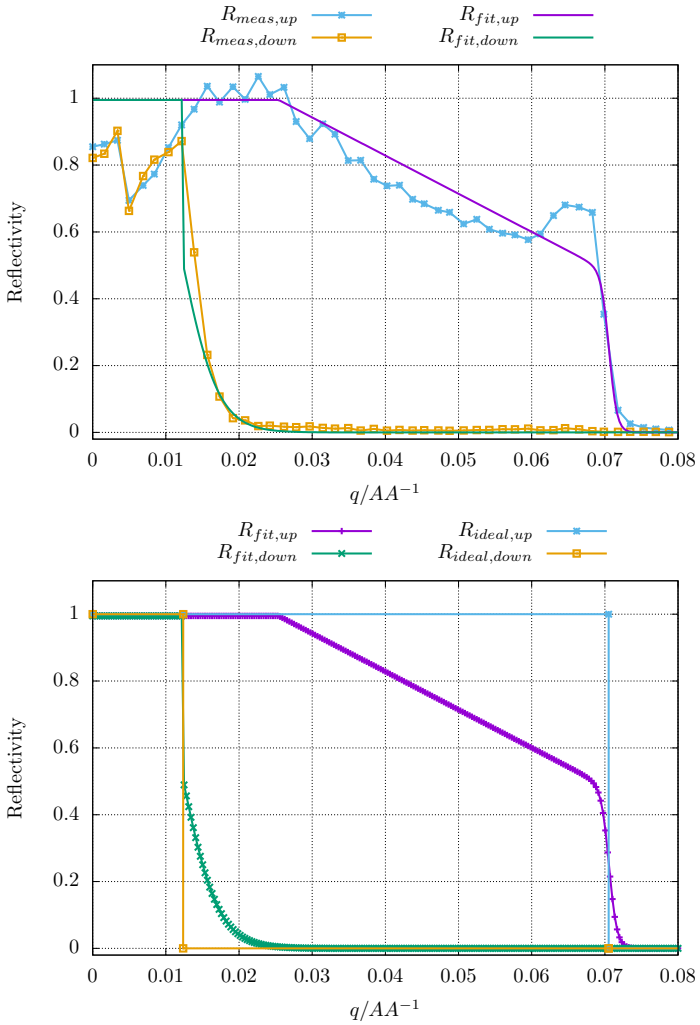

Figure 6: Top: Measured neutron reflectivity of the coating on the blades of the PSI-prototype analyzer for spin-up (blue) and spin down (yellow) neutrons. N.b. in some cases the reflectivity > 1, which is clearly unphysical. Also fits to the measurements: purple and green for up and down respectively. Bottom: The fitted curves with an idealized set for testing where cut-offs have been matched to the fits (blue and yellow)

- Above the transition wavelength there is a range (again for the real reflectivity curves) where the polarization is $P_y < 0$. This is easily understood since the reflectivity for spin-down is somewhat higher than for spin-up, e.g. $R_{down} - R_{up}|_{q<0.008} \approx 0.05$

For the remainder of this section, the reflectivities from fig. 6 will be referred to as ideal and real or measured reflectivity, respectively.

4.2 BOA experiment simulation

The next step in the component testing was to insert the MAGiC analyzer prototype in a real beamline - in this case the testing beamline BOA at PSI, where C. Klauser has already performed some test measurements. The experiment was set up along the lines of the sketch show in fig. 9, and a simulation was designed to mimick this as closely as possible. This simulation beamline is quite detailed in terms of the upstream guide system, and also includes a model of the double bounce monochromator used at BOA. There is some uncertainty wrt. to the monochromator and what it actually contains, but this is likely of less concern for our purposes.

Turning to (a model of) the 2D-area detector used at BOA for the measurements, we now examine the spatial distribution of the beam transmitted through the analyzer. This is shown in fig. 10. Two peaks appear at $x = 0$ and 1.5 cm. Upon closer inspection using the `bounce` output parameter of the analyzer component. We find the central peak to arise from neutrons that have been reflected twice, whereas the right-hand peak arises from triple-reflections. This could potentially be a serious problem, as it could lead to entangling peaks coming from different scattering processes.

4.3 Reflection order study

To further investigate this issue we proceed to set up a test simulation using only a source focusing on the single blade in the centre of the analyzer (for simplicity). Figure 11 shows intensity in several reflection orders while increasing the size of the model source (corresponding to scanning the middle slit in fig. 9). As expected, when the source gets larger thereby increasing the available divergence we allow more reflection orders. For the set up with the slit at 1 mm only 2nd and 3rd order reflections are possible. To verify that the component is working correctly we may replace the analyzer blade with a rotated guide. Qualitatively this is in contrast to what was seen experimentally at BOA, where only the 3rd order was found. A possible explanation for this is that the divergence profile of BOA at the middle slit is neither uniform, nor symmetric along the beam width.

Let a wide source (20 mm wide) illuminate the analyzer prototype through a 1mm wide slit, and scan the slit across the source width. The results are as expected from geometrical considerations: A given reflection order may be triggered by a certain range of divergence and hence position of the slit. Similar

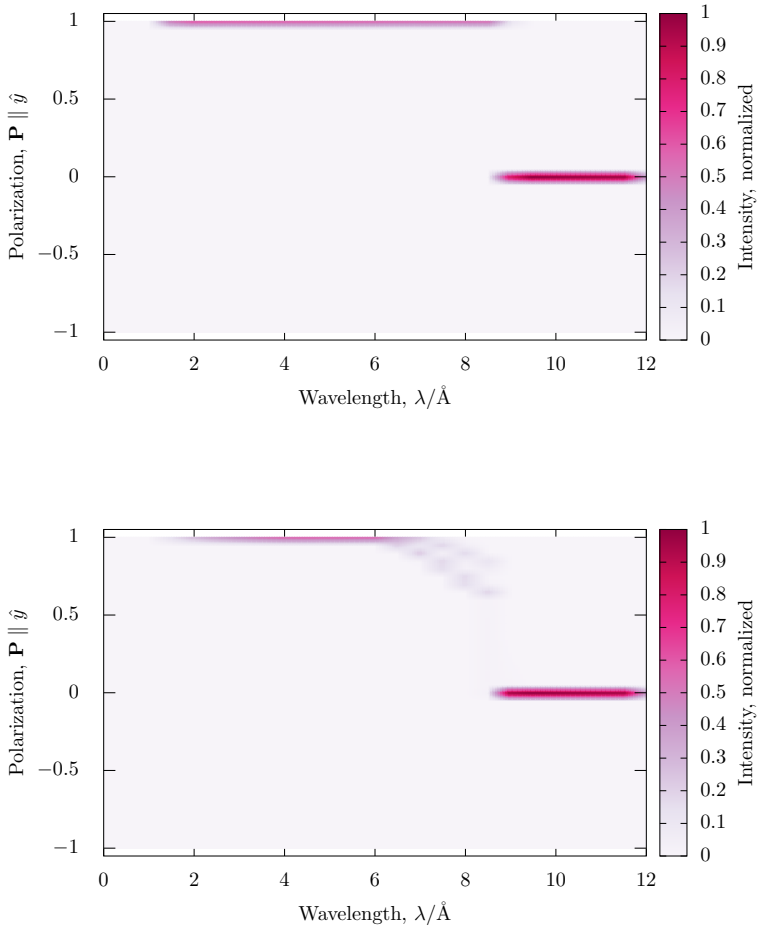

Figure 7: Polarization along the Y-axis as a function of wavelength for the simulated PSI-prototype (parameters in table 1) using: (Top) an idealized square reflectivity curve, and (bottom) the measured reflectivity (fig. 6), for an unpolarized incident beam with a flat wavelength spectrum.

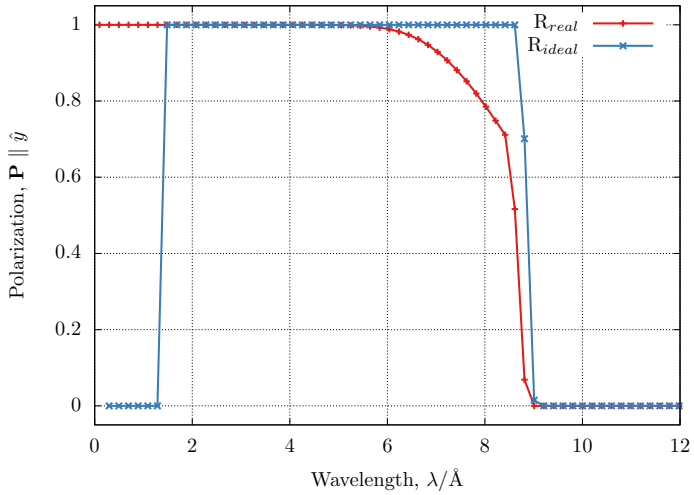

Figure 8: Mean polarization along Y-axis vs. wavelength. for the simulated PSI-prototype, with fitted reflectivity (R_{real}) and idealized R_{ideal} reflectivity (fig. 6).

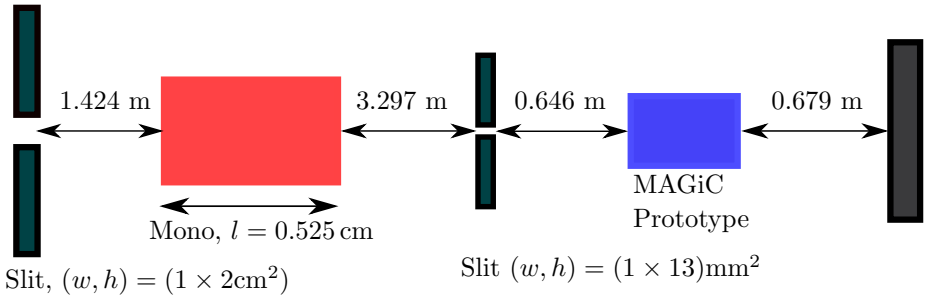

Figure 9: Simplified sketch of the experimental set up at BOA. N.b. this sketch does not include the upstream guide system, which was included in the simulations.

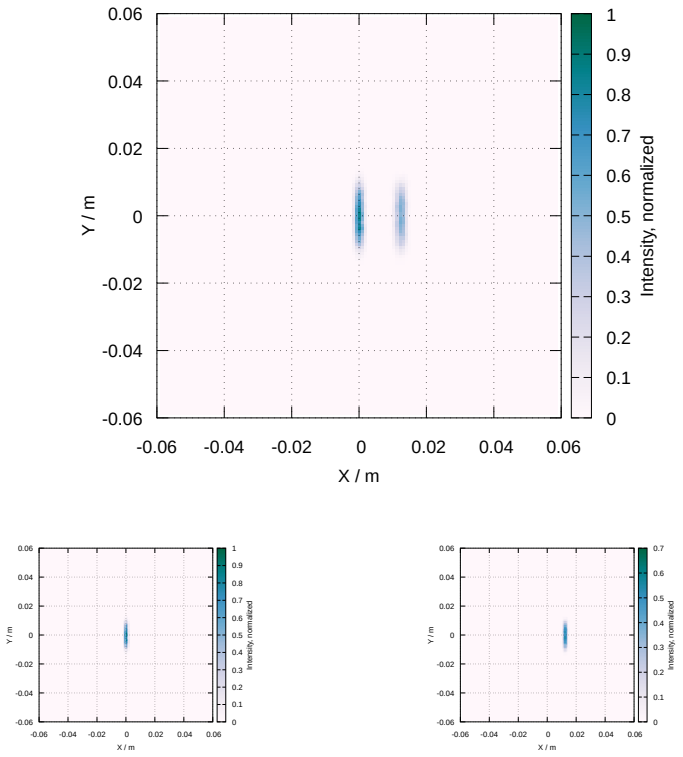

Figure 10: Spatial distribution of intensity after the prototype analyzer at BOA with the monochromator set to 3.5 Å. Top: complete intensity, Bottom Left: Only thos neutrons twice reflected, Bottom Right: Only neutrons thrice reflected.

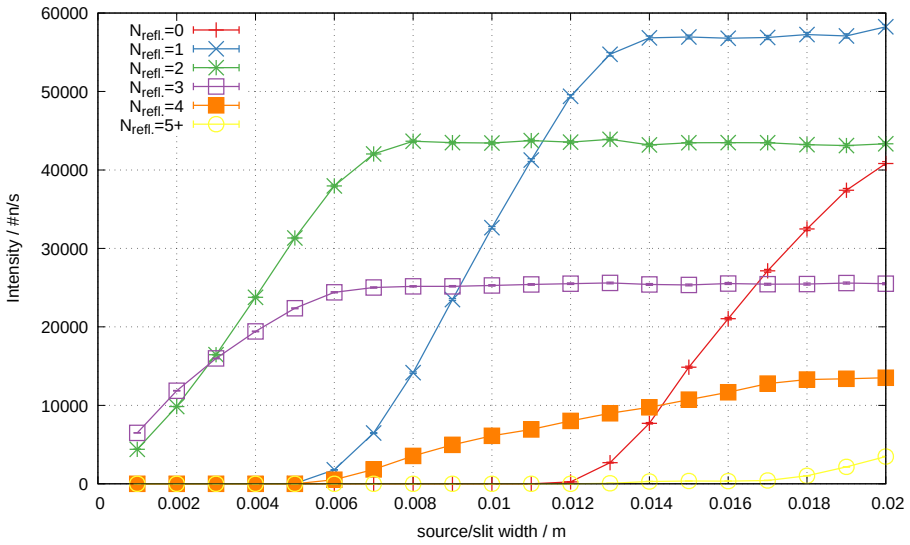

Figure 11: Intensity as a function of source size for a model source illuminating only the central blade of the prototype analyzer with $\lambda \approx 4\,\text{Å}$ neutrons, for a set of reflection orders, N. $N = 5+$ means 5 or more reflections.

to fig. 11, fig. 12 shows the intensity of reflection orders but as a fucntion of slit position. Clearly, a parameter interval is found: source x-position: $x_0 \approx 2.5\,\text{mm}$ where almost all intensity transmitted by the analyzer comes from the 3rd order reflection. A likely explanation for the experimental results is simply a misalignment of the middle slit on the order of mm. In this way this effect is highly connected to misalignment studies. Also, and perhaps more seriously, it would limit the effective sample-size accessible with the device.

4.4 Full sample modelling and resolution

MAGiC is intended for PA use with sample size up to 2 mm radius. It is therefore of interest to determine whether the proposed geometry of a solid state analyzer will give rise to peak splitting from a standard sample. Using the sample models included in McStas we may quite simply insert a sample and examine relevant peaks and their contributions from the different scattering orders. At MAGiC the detector position has been fixed at a distance of 1.005 m from the sample centre. Scattering from a Na2Ca3Al2F14-powder with library parameters[] on an idealized banana-shaped monitor at this distance is shown in fig. 13. From this we fit Gaussians peaks to a randomly chosen peak at $2\theta \approx -45.5°$., and find that the fits show similar peak widths: 0.057° for the solid state device (MAGIC) and 0.052° for the adapted bender (FOCUS adapted).

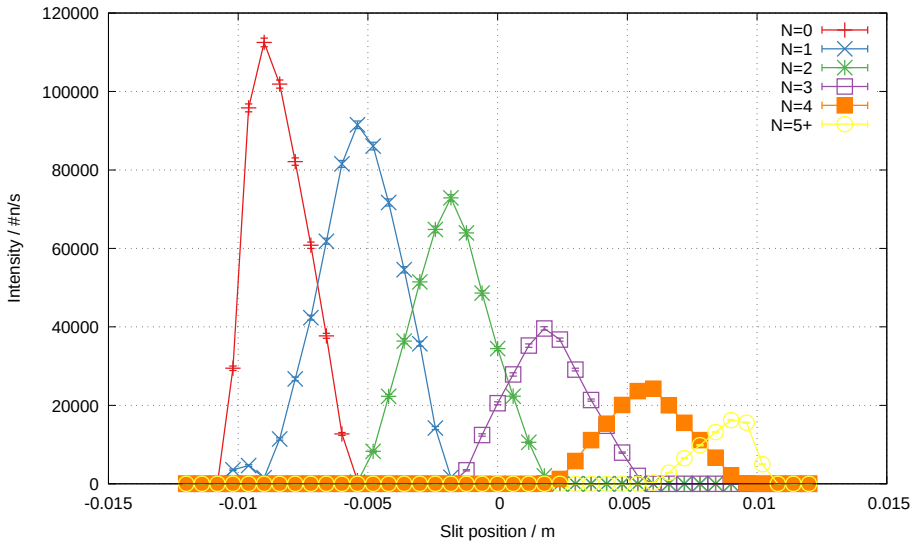

Figure 12: Intensity reflected and/or transmitted (i.e. not absorbed) in the PSI prototype analyzer when illuminated by a flat source, with a 1mm wide slit moving along the source width in front of it.

5 Analyzer comparisons

To put the analyzer into context and get reference points for its performance we compare the proposed PSI Solid State analyzer (referred to as Solid State device or simply S/S) with 2 similar devices based on a the curved bender concept, as found on the SNS HYSPEC instrument, and on the PSI FOCUS instrument. The parameters for the 3 analyzer versions shown in table 3. The HYSPEC analyzer is a direct copy of the analyzer installed at the SNS instrument HYSPEC[3]; FOCUS (adapted) refers to a bender analyzer whose basic parameters are identical to what is found on the PSI instrument FOCUS, but its geometry has been adapted to fit the space allotted to the analyzer at MAGiC. For instance the geometry has been adjusted such that it ends on the same curvature as the Solid state device would do (a radius of 0.9 m).

In all the following the sample is identical to before: A cylindrical sample with a radius of 2 mm, where only the incoherent cross section is significant. The scattered beam is fully unpolarized. This procedure isolates the analyzer performance from any other effects and provides a clear comparison.

We see in fig. 14 that for wavelengths: $\lambda > 0.5\,\text{Å}$ the transmission rises sharply, while polarization falls. This merely reflects that the analyzer is operating in the regime where both spin states are reflected. Naturally, this increases the transmission and decreases polarization.

We conclude (unsurprisingly) from fig. 14 that the unmodified HYSPEC-clone analyzer is clearly inferior to both the Solid State device and the adapted

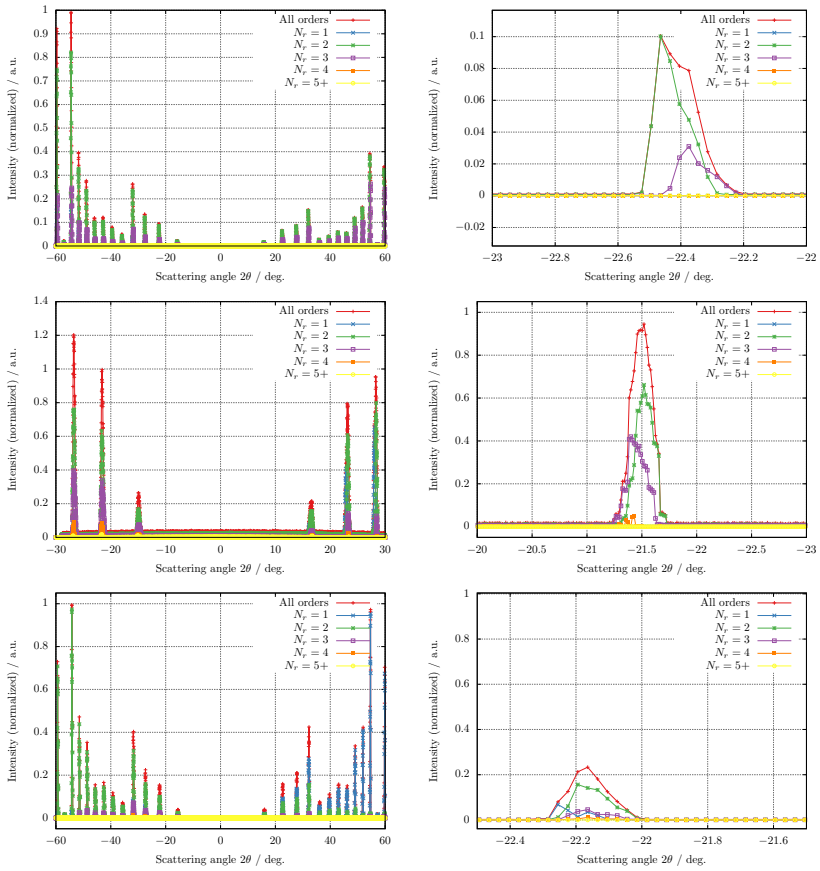

Figure 13: Simulated powder scattering from a NaCaAlF-powder as recorded on a banana-shaped screen with a single row of pixels. The signal travels through the wide angle analyzer on. The left hand side shows a full range of peaks within the acceptance angle of the analyzer. On the right are closeups on a single peak to clearly resolve the different orders of reflection. Top row: proposed MAGiC solid state analyzer; middle row: clone of HYSPEC analyzer; bottom row: FOCUS-like analyzer, adapted to the MAGiC geometry.

Analyzer:	MAGIC S/S	HYSPEC	FOCUS (adapted)
coverage / °	120	60	120
bend radius / m	-	4.6	4.8
channel width / m	0.150×10^{-3}	0.4×10^{-3}	0.4×10^{-3}
blade length / m	0.04	0.171	0.14
entry radius. / m	0.9	0.55	0.8
# channels	10500	960	2760

Table 3: Parameters for the 3 compared wide angle analyzers. MAGiC S/S refers to a solid state device, whereas HYSPEC and FOCUS (adapted) are bend channel devices. HYSPEC is a direct copy of the device installed at the SNS instrument with same name. FOCUS (adapted) is based on the parameters of the analyzer installed at the PSI instrument, but adapted to fit at the MAGiC.

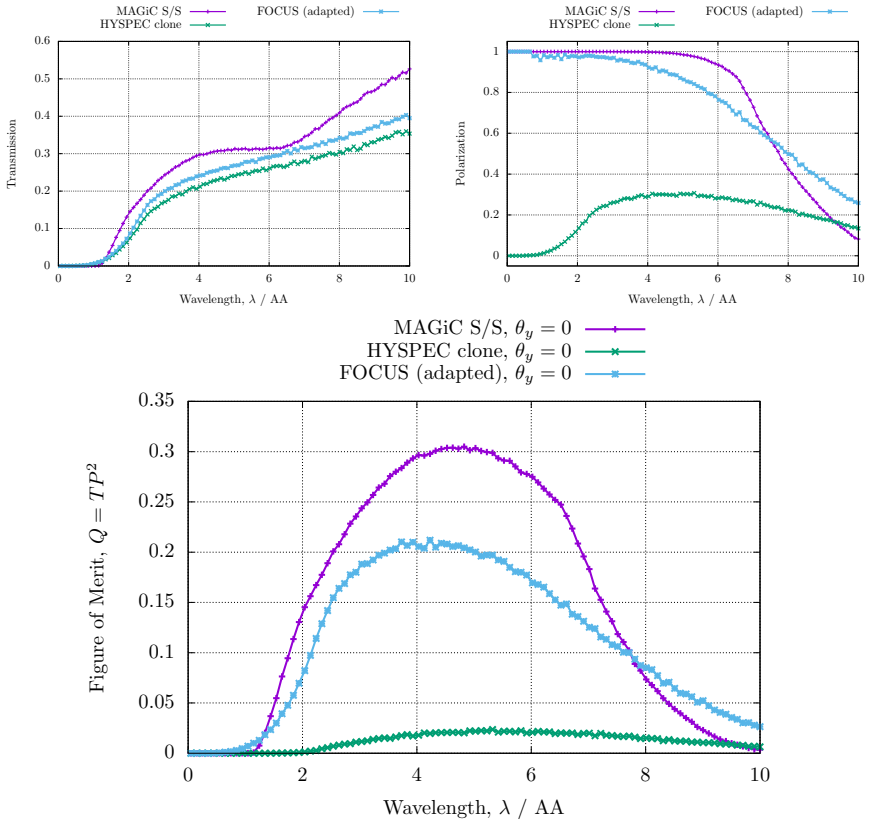

Figure 14: Performance of three analyzer devices in terms of Transmission, T (top, left); Polarization power: P (top right); and polarizer figure of merit: $Q = TP^2$ (bottom). In all 3 cases, the analyzers are driven by an unpolarized beam with $\lambda \in [0:10]$Å, scattering on a purely incoherent (isotropic) scatterer.

FOCUS analyzer. Henceforth we will therefore limit our comparisons to these two devices.

5.1 Misalignment

In this section we present a set of studies of robustness of the analyzer in terms of misalignment of the analyzer.

We study the effect of misaligning the complete analyzer housing. Using McStas - this can be done using a simple ROTATED-statement on the analyzer. Figure 15 shows the polarizer figure of merit $Q = TP^2$ as a function of wavelength, for some different conditions for the two types of analyzers adapted for MAGiC. Clearly (as expected) the most sensitive rotation axis is the (vertical) y-axis, whereas the performance characteristics change significantly with a misalignment of 0.1° for the solid state analyzer, we see no such change for the bender analyzer. Consider for example 6 Å neutrons impinging on a 0.1° misaligned solid state analyzer. This could then lead to a drop in performance by $\approx 60\%$. The misalignment manifests itself as a change of the operational wavelength range of the analyzer. The high loss of performance is then due to the particular wavelength ending up outside the range. Rotations around the other two axes are much less significant. We therefore conclude that both types of analyzer would be relatively straight forward wrt. misorientation around X and Z, whereas alignment around Y must be controlled carefully for a solid state analyzer. Extending the supermirror coating to a higher m-value, thereby shifting the cut-off towards higher q, results only in very minor improvement of the operating wavelength range towards short wavelengths, as the reflectivity is already . If on the other hand the slope α could be improved that would have an significant impact. Towards long wavelengths the range is bounded by the difference between $q_{c,up}$ and $q_{c,down}$, which is fixed by material choice.

6 Full MAGiC analyzer simulation

All in all, we now turn to adding the analyzer into the updated model of MAGiC as received from lead scientist X. Fabreges (LLB). Figure 16 shows 3D-views of the model thus created, which includes a sample model using the union-concept. The MAGiC instrument model complete analyzer and polarizer options works as expected, with no additional conclusions drawn immediately wrt. the solid state analyzer. The detector surface is sufficiently close to the analyzer exit to avoid reflection order problems etc.

7 Conclusions

From all these deliberations we may draw some conclusions:

- The Solid state device shows overall better basic performance in terms of of both transmission and Polarizing power, (and hence in $Q = TP^2$) than

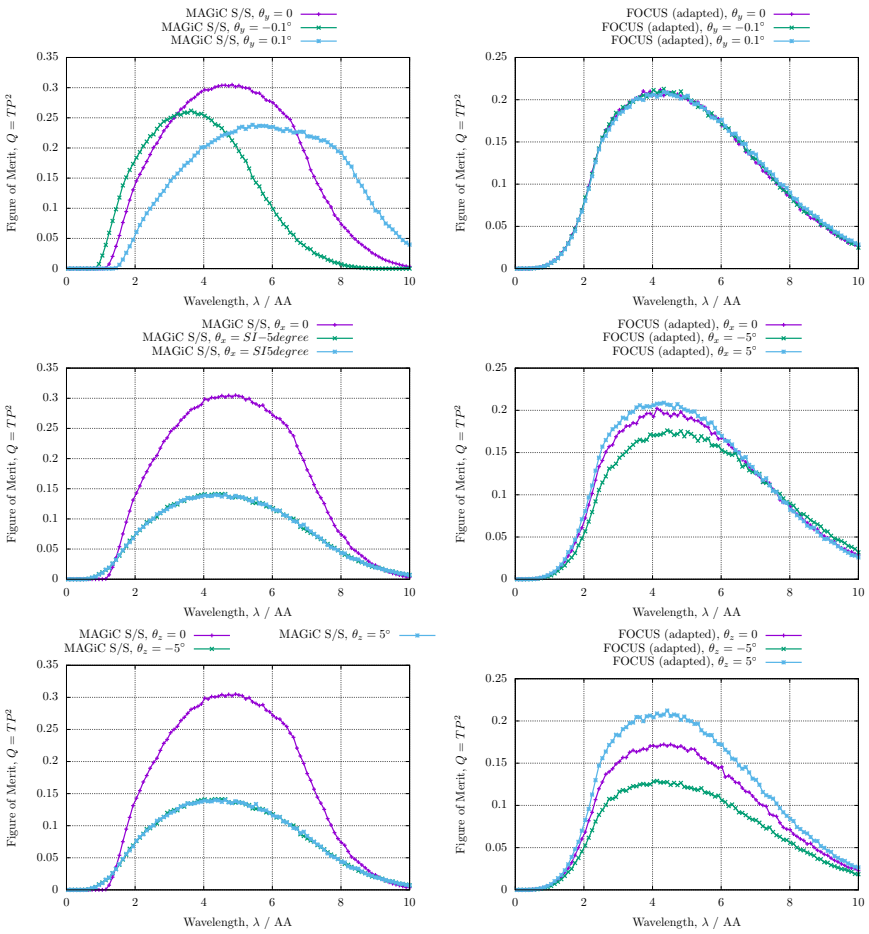

Figure 15: Misalignment scans for the adapted FOCUS device and the MAGiC solid state analyzer. The analyzer device is rotated by an amount around the principal axis in turn. with the centre of its entry arc as its pivot point. Rotation is around the z-axis (top left), x-axis (top right), y-axis for the MAGiC solid state (bottom left), and y-axis for the adapted FOCUS bender analyzer. The analyzers are robust against misalignment around z and x. The solid state device on the other hand is very sensitive to misorientation in the XZ-plane (around the y-axis).

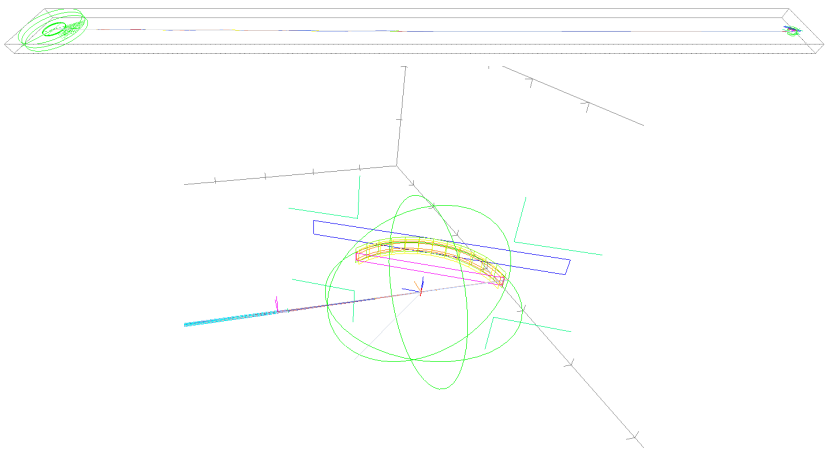

Figure 16: 3D-views of the full MAGiC instrument model. The top image shows an overview of the complete instrument, the lower image shows a close-up of the sample area. The analyzer is drawn in orange

a comparable bender device. The Focus -style device shows roughly 30 % less in performance.

- If the detector is close to the analyzer exit as is the case for MAGiC, reflection order-mixing section 4.3 is not an issue.
- A high valued and uniform reflectivity curve directly translates into a uniform Quality factor.
- The solid state analyzer is sensitive to rotational misalignment around the vertical axis, and can lead to significant performance loss (section 5.1) of as much as 60 %. Predominantly the effect will be that the operational wavelength range is shifted, meaning that the wanted wavelength can end up beyond cut-off.
- In terms of angular resolution the devices show similar performance.

The leads us to conclude that in terms of nominal performance, the proposed solid state device is the better choice for MAGiC, but It should be stressed that this conclusion is arrived at without taking *any* manufacturing and/or engineering considerations into account. The advantage of using the solid state bender can easily be lost if the device is misaligned, as this must be considered an uncontrolled parameter. If a precision of 0.1° around the vertical axis is not likely to be reached, this study suggests a bender type device.

A further analysis should also be done in terms of misalignment of single blades inside the analyzer, as well as misaligned analyzer blocks wrt. each other, if it cannot be built as a single entity.

References

[1] Rodion Kolevatov. "McStas and Scatter Logger driven calculations of prompt gamma shielding for neutron guides". In: *Journal of Neutron Research* Preprint (2019), pp. 1–7.

[2] P. Willendrup et al. "McStas: Past, present and future". In: *Journal of Neutron Research* 17.1 (2014). ISSN: 14772655. DOI: 10.3233/JNR-130004.

[3] Igor A Zaliznyak et al. "Polarized neutron scattering on HYSPEC: the HYbrid SPECtrometer at SNS". In: *J. Phys. Conf. Ser.* Vol. 862. 2017, p. 012030.